BNL-224980-2023-TECH

EIC-ADD-TN-078

Beam-induced heat deposited in the EIC HSR screens

S. Verdu-Andres

September 2023

Electron-Ion Collider

Brookhaven National Laboratory

U.S. Department of Energy

USDOE Office of Science (SC), Nuclear Physics (NP) (SC-26)

DISCLAIMER

Beam-induced heat deposited in the EIC HSR screens

Silvia Verdú-Andrés* and Medani Sangroula
Brookhaven National Laboratory
Upton, NY 11973 (USA)
(EIC Project)
(Dated: September 27, 2023)

The beam screens of the Electron-Ion Collider (EIC) Hadron Storage Ring (HSR) have several beam-induced heat sources: the resistive-wall impedance, the electron cloud, and beam particle losses. This note discusses the heat load to the HSR screens from resistive-wall impedance and beam particle losses for different beam scenarios.

I. INTRODUCTION

Every superconducting magnet from the Relativistic Heavy Ion Collider (RHIC) used in the Hadron Storage Ring (HSR) arcs of the Electron-Ion Collider (EIC) will be equipped with a beam screen [1]. The screens feature a thin film of amorphous carbon on top of a high RRR copper clad stainless steel wall. The screens have a cooling pipe with flowing helium that will keep the temperature of the screens below 10 K. The heat load to this cooling circuit is contributed, among other components, by the screens. The screens have several beam-induced heat sources: the resistive-wall impedance, the electron cloud, and beam particle losses. This note summarizes the heat load to the HSR screens from resistive-wall impedance and beam particle losses for different beam scenarios.

II. RESISTIVE-WALL IMPEDANCE

The resistive-wall heat deposited in the screen by the beam depends on the beam scenario via $\mathrm{Q}^2\mathrm{M}/\sigma_\mathrm{t}^{3/2}$ (factor F_QMS in Table I, see Eq. 3 in Ref. [1]); the operation mode (beams run on-axis during store and off-axis in collision mode, with the offset being dependent on the beam energy and the type of the magnet hosting the screen, with the largest offset at quadrupoles and sextupoles) and the screen location (the magneto-resistance featured by the copper layer depends on the magnet strength; the beam offset is not constant along the ring lattice [2]). The resistive wall heating per unit length $\mathrm{P'_{RW}}$ has been accordingly parameterized as follows:

$$P'_\mathrm{RW} = F_\mathrm{QMS}[Q, M, \sigma_t]\times \left(P'_\mathrm{Cu}[x] \times \frac{F_\mathrm{MR}[RRR, B] \times F_\mathrm{ASE}[RRR, \sigma_t]}{\sqrt{RRR}} + P'_\mathrm{SS}[x] \right) \quad (1)$$

where $P'_\mathrm{Cu}[x]$ and $P'_\mathrm{SS}[x]$ are, respectively, the resistive-wall heating in room-temperature copper and stainless steel surfaces by the proton beam for the highest E_CM scenario with horizontal offset x. The impact of magnetoresistance (MR) and its dependence on the magnetic field B and the copper RRR is included in factor F_MR. The impact of the anomalous skin effect (ASE) and its dependence on the copper RRR and the beam spectrum is incorporated in factor F_ASE. The value of these two factors is provided in Ref. [3]. The contribution of the thin amorphous carbon layer to the beam-impedance of the screen is negligible.

A. Resistive-wall heating evaluations

The most recent screen design incorporates an array of pumping slots for dynamic pressure stability. The pumping slots are opened in the flat walls of the screen. Beam-induced radio-frequency fields can leak through the pumping slots, reaching the outer wall of the screen, its cooling channel and the beam pipe, all with stainless steel surfaces. The model used to compute the resistive-wall heating in the different components is shown in Fig. 1, and includes the stainless steel beam pipe, the stainless steel cooling channel, and the screen divided into two concentric volumes: an outer volume to compute the losses in the stainless steel surface of the screen and an inner one for losses in the copper surface.

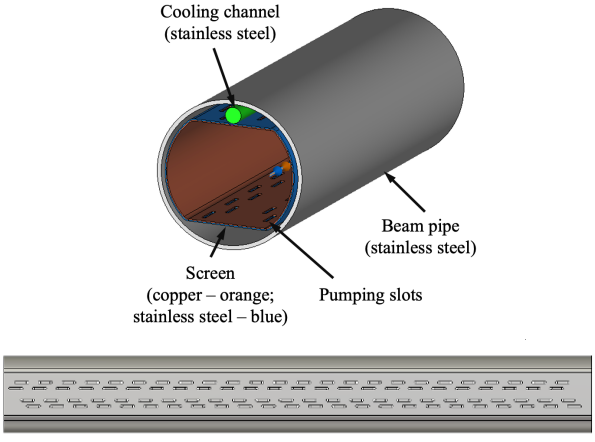

FIG. 1. Model used to compute resistive-wall heating (top) and top view of screen with array of pumping slots (bottom).

* Corresponding author: sverdu@bnl.gov

The baseline manufacturing strategy plans for the screens to be fabricated from a single piece, with only one longitudinal weld required to close the screen profile. To avoid any contamination of copper into the stainless steel weld – which could jeopardize the mechanical strength of the weld – the copper layer is removed at both sides of the weld joint. This will expose a 2 mm-wide strip of stainless steel to the beam. Two different weld locations are studied in detail. First, a weld located in the curved wall, 6 mm below the flat wall. Second, a weld at the center of one of the flat walls. Our impedance evaluations assume that the longitudinal weld is flat, with negligible bead height.

The resistive-wall heating dependence on beam offset in the copper surface is comparable for both weld locations, increasing as the beam approaches the curved wall. As the beam offset increases, the resistive-wall heating in the surface of the weld located in the curved wall increases, reaching a maximum and later decreasing. This is attributed to the fact that as the beam offsets, the beam-induced currents concentrate in the middle plane of the curved wall. For the weld located at the center of the flat wall, the resistive-wall heating decreases as the beam offset increases, that is, as the beam moves away from the weld. Figures 2 and 3 show, respectively, the resistive-wall heating at the stainless steel weld strip and the copper surfaces by the proton beam for the highest $E_{\rm CM}$ scenario when the weld is located on the curved wall. Fig. 4 and 5 show the resistive-wall heating at the stainless steel weld strip and the copper surfaces by the proton beam for the highest $E_{\rm CM}$ scenario when the weld is located at the center of one of the flat walls. Coefficient values for the polynomial fits to the resistive-wall heating dependence on the beam offset, $P'[x]$, are listed in Tables II and III for the two weld locations studied. The resistive-wall heating of the cooling channel and beam pipe is in the order of W/m, negligible in comparison to the losses in the other components. The model used to evaluate the resistive-wall heating for the weld located in the curved wall did not have pumping slots. The heat deposited in the screen increases by 0.02 W/m due to RF fields leaking through the pumping holes and reaching the stainless steel outer wall of the screen.

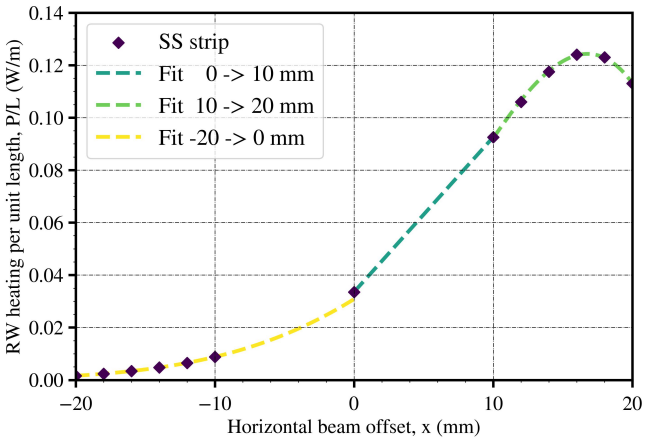

FIG. 2. Resistive-wall heating per unit length in the stainless steel weld strip in the curved wall by the highest $E_{\rm CM}$ 275 GeV proton beam. Calculated for electrical conductivity of stainless steel at room temperature, $\sigma_c = 1.35 \times 10^6$ S/m. The points are fit by the polynomials in Table II. Zero beam offset in the vertical coordinate.

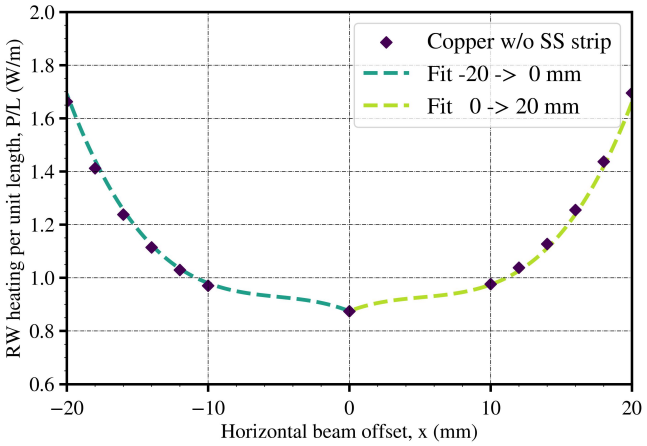

FIG. 3. Resistive-wall heating per unit length in the copper surface of a racetrack screen by proton beam for the highest $E_{\rm CM}$ scenario. Calculated for electrical conductivity of copper at room temperature, $\sigma_c = 5.8 \times 10^7$ S/m. The points are fit by the 3rd order polynomials given in Table II.

B. *Example:* Resistive-wall heating in an arc dipole screen by proton beam for the highest Ecm scenario circulating in collision orbit

Assume the beam screen with weld in a curved wall, inside an arc dipole, with the highest Ecm beam (275 GeV protons, 60 rms mm-long bunches, 290 bunches, 19.1×10^{10} protons per bunch) circulating in collision mode at x = -21 mm offset (the minus sign indicates that the stainless steel weld strip is in the opposite side to the beam offset): $P'_{\rm SS}$[-21 mm] = 0.0013 W/m and $P'_{\rm Cu}$[-21 mm] = 1.8437 W/m, respectively, from Fig. 2 and Fig. 3. For RRR 100 copper, $F_{\rm MR} = 1.44$ in the arc dipoles from Table III and IV in Ref. [3] and $F_{\rm ASE} = 1.50$ from Fig. 11 also in Ref. [3], so $P'_{\rm RW} = 0.40$ W/m (see Fig. 6). For RRR = 50, $P'_{\rm RW} = 0.47$ W/m. In comparison, $P'_{\rm RW} = 0.16$ W/m for the 100 GeV proton beam with RRR 100 copper (2.6 times lower), despite being closer to the stainless steel weld strip (x = 21 mm) in collision mode. For screens with one longitudinal weld, ideally the weld shall be placed in the curved wall opposite to the orbit of the colliding 275 GeV proton beam. The colliding 100 GeV proton beam runs closest to this wall, but deposits 2.6 times less heat than the 275 GeV highest $E_{\rm CM}$ beam. As result, the heat deposited by the 100 GeV beam onto the screen and the stainless steel

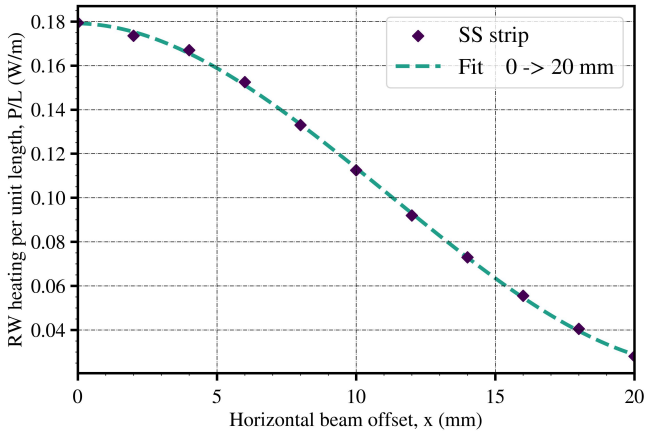

FIG. 4. Resistive-wall heating per unit length in the stainless steel weld strip in the flat wall by the highest E_{CM} 275 GeV proton beam. Calculated for electrical conductivity of stainless steel at room temperature, $\sigma_c = 1.35 \times 10^6$ S/m. The points are fit by the polynomials in Table III. Zero beam offset in the vertical coordinate.

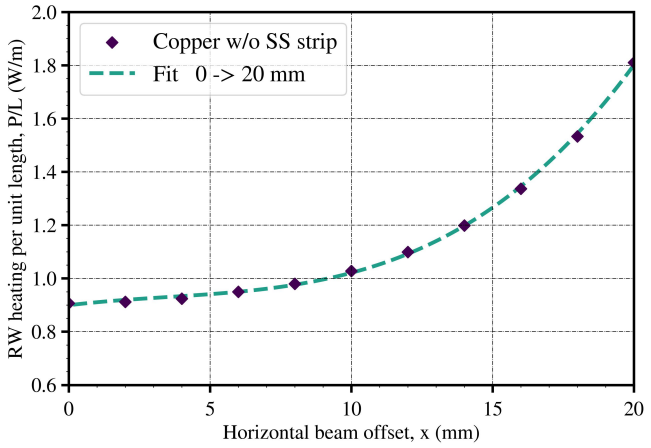

FIG. 5. Resistive-wall heating per unit length in the copper surface of a racetrack screen by proton beam for the highest E_{CM} scenario. Calculated for electrical conductivity of copper at room temperature, $\sigma_c = 5.8 \times 10^7$ S/m. The points are fit by the 3rd order polynomials given in Table II.

strip will still be smaller than the heat deposited by the 275 GeV beam. However, placing the weld in the flat wall helps to reduce the heat load dependence on beam offset, as seen in Fig. 7.

III. ELECTRON CLOUD

The heat load contributed by electron cloud is discussed in Ref. [5] and Ref. [1].

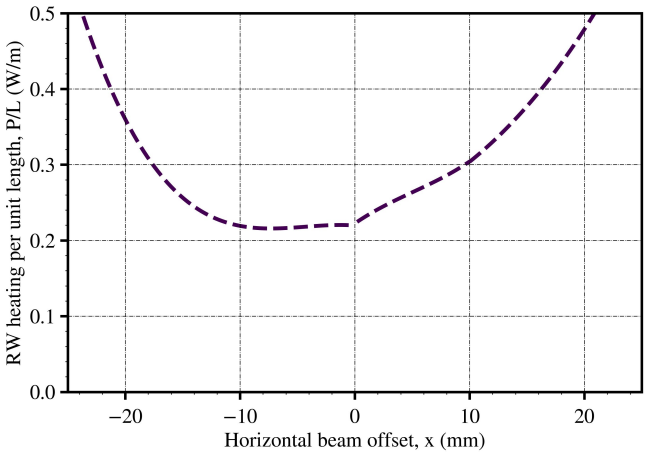

FIG. 6. Resistive-wall heating per unit length in racetrack screen (RRR 100 copper surface plus stainless steel weld strip in curved wall) of arc dipoles by the highest E_{CM} 275 GeV proton beam (includes magneto-resistance and anomalous skin effect contributions). Zero beam offset in the vertical coordinate.

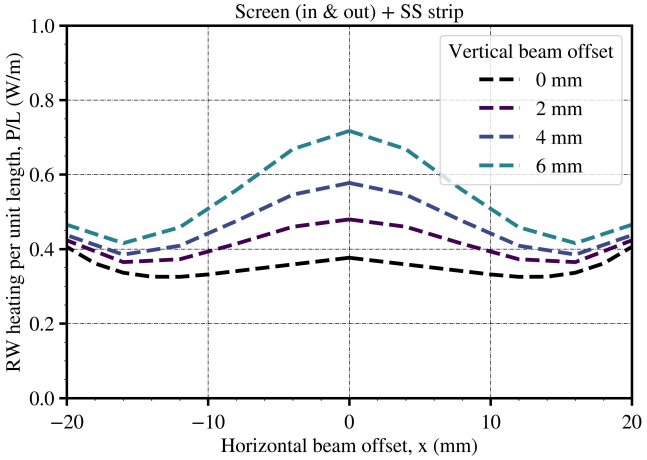

FIG. 7. Resistive-wall heating per unit length in racetrack screen (RRR 100 copper surface plus stainless steel weld strip in flat wall) of arc dipoles by the highest E_{CM} 275 GeV proton beam (includes magneto-resistance and anomalous skin effect contributions) for different beam offsets.

IV. BEAM PARTICLE LOSS

The heat load from beam particle losses is estimated assuming a uniformly distributed particle loss along the circumference of the EIC HSR in one beam lifetime. The beam lifetime τ is defined as the time it takes to reduce particle population to 1/e of its initial value:

$$dN = -\alpha N(t)dt \text{ where } \alpha = \text{constant} \quad (2)$$

$$N = N_0 \exp -t/\tau \text{ where } \tau = 1/\alpha \quad (3)$$

In one lifetime, 63% of the particles are lost (1-1/e = 0.63). For a uniformly distributed particle loss along the

circumference of the EIC HSR (3833.45 m), the heat due to particles lost in one lifetime is calculated as:

$$P'_{\mathrm{PL}}[\mathrm{W/m}] = U \times 0.63/\tau[s]/3833.45\ \mathrm{m} \quad (4)$$

with U being the stored energy in the beam:

$$U = MNqV \quad (5)$$

where M is the number of bunches, N is the number of particles per bunch and qV is the beam energy. In that regard, the proton beam for the highest $\mathscr{L}$ scenario (1160 x 6.9e10 ppb) is 1.45 times more energetic than the proton beam for the highest E_{CM} scenario (290 x 19.1e10 ppb). Taking the proton beam for the highest $\mathscr{L}$ scenario and τ = 10 h, U = 3.52 MJ and P'$_{\mathrm{PL}}$ = 0.016 W/m. For the highest E_{CM} scenario proton beam, P'$_{\mathrm{PL}}$ = 0.011 W/m.

V. CONCLUSIONS

This note summarizes the heat load to the HSR screens from resistive-wall impedance, including the contribution of the longitudinal weld seam, and beam particle losses for different beam scenarios.

ACKNOWLEDGMENTS

We are grateful to Charlie Hetzel and Brian Gallagher (BNL) for providing screen models and useful feedback.

[1] S. Verdú-Andrés, Electron cloud thresholds at the arcs of the Electron-Ion Collider hadron storage ring, Tech. Rep. EIC-ADD-TN-065; BNL-224588-2023-TECH (2023).
[2] G. Robert-Demolaize, Private communication (May 16, 2022).
[3] S. Verdú-Andrés, Beam-impedance considerations for the EIC HSR screen. Tech. Rep., (2023), under preparation.
[4] V. Ptitsyn, eRHIC parameter table v.6.
[5] X. Gu, A. Blednykh, M. Blaskiewicz, G. Robert-Demolaize, and S. Verdu-Andres, Electron Cloud Simulations for the Electron-Ion Collider in Brookhaven National Laboratory, Tech. Rep. EIC-ADD-TN-053; BNL-224221-2023-TECH (2022).

TABLE I. Proton beam parameter values for different EIC beam scenarios [4].

Beam scenarios	275 GeV p + 18 GeV e (Highest E_{CM})	275 GeV p + 10 GeV e (Highest $\mathscr{L}$)	100 GeV p + 10 GeV e	100 GeV p + 5 GeV e	41 GeV p + 5 GeV e
Energy (GeV)	275	275	100	100	41
No. bunches, M	290	1160	1160	1160	1160
Bunch spacing (ns)	40.59	10.15	10.15	10.15	10.15
Bunch charge, Q (10^{10})	19.1	6.9	6.9	4.7	2.6
RMS bunch length, σ_s (cm)	6	6	7	7	7.5
$F_{QMS} = Q^2M/\sigma_t^{3/2}$ (a.u)	1	1/2.0	1/2.6	1/5.7	1/20

TABLE II. Coefficient values for polynomial fit to the resistive-wall heating P' dependence on beam offset (x, y), with P' $[x] = C_3\ x^3 + C_2\ x^2 + C_1\ x + C_0$ for screen with copper inner wall and stainless steel weld strip at room temperature. Screen without pumping holes. Weld located at curved wall, 6 mm away from flat wall.

	Fit range, x (mm)	C_3	C_2	C_1	C_0
Inner wall	[0,20]	1.99627772e-04	-3.06044191e-03	2.06150868e-02	8.74304263e-01
	[-20,0]	-2.04259047e-04	-3.09622172e-03	-2.11030549e-02	8.74314031e-01
Weld strip	[0,10]	-3.77245917e-05	9.44310896e-04	1.85840314e-04	3.35154781e-02
	[10,20]	0	0	0.0059	0.0335
	[-20,0]	1.79398148e-06	1.27827381e-04	3.29907407e-03	3.07968254e-02

TABLE III. Coefficient values for polynomial fit to the resistive-wall heating P' dependence on beam offset (x, y), with P' $[x] = C_3\ x^3 + C_2\ x^2 + C_1\ x + C_0$ for x $\in [0, 20]$ mm for screen with copper inner wall, stainless steel outer wall and stainless steel weld strip at room temperature. Screen with pumping slots. Weld located at the center of the flat wall.

	y (mm)	C_3	C_2	C_1	C_0
Inner wall	0	2.05228124e-04	-3.05016181e-03	2.17595671e-02	8.84559515e-01
Outer wall		7.50267231e-07	-5.86773328e-05	1.92969104e-04	2.03997629e-02
Weld strip		2.17400092e-05	-7.34317917e-04	-1.57336351e-03	1.79516849e-01
Inner wall	2	1.65798611e-04	-1.67261905e-03	1.11591270e-02	8.81209524e-01
Outer wall		2.89351852e-07	-4.75198413e-05	1.54497354e-04	2.07301587e-02
Weld strip		4.34027778e-05	-1.36994048e-03	-1.60039683e-03	2.68295238e-01
Inner wall	4	1.75520833e-04	-1.90535714e-03	1.23630952e-02	9.13571429e-01
Outer wall		5.78703704e-08	-4.86111111e-05	2.10185185e-04	2.22888889e-02
Weld strip		6.19791667e-05	-1.86250000e-03	-3.42023810e-03	3.58085714e-01
Inner wall	6	1.95428241e-04	-2.31775794e-03	1.47703704e-02	9.78406349e-01
Outer wall		1.28538196e-20	-6.51785714e-05	5.03571429e-04	2.46571429e-02
Weld strip		8.88888889e-05	-2.51666667e-03	-7.08412698e-03	4.82419048e-01